Induction of viral mimicry upon loss of DHX9 and ADAR1 in breast cancer cells

Kyle A. Cottrell [1,4,5‡*], Sua Ryu [1,4‡], Luisangely Soto Torres [1,4], Angela M. Schab [1,4], Jason D. Weber [1,2,3,4*]

[1]Department of Medicine, Division of Molecular Oncology, [2]Department of Cell Biology and Physiology, and [3]Department of Biology, Siteman Cancer Center, [4]ICCE Institute, Washington University School of Medicine, Saint Louis, Missouri, USA

[5]Department of Biochemistry, Purdue University, West Lafayette, IN, USA

‡ Authors contributed equally

*Co-Corresponding authors

Correspondence:
Kyle A Cottrell, Ph.D.
Department of Biochemistry
Purdue University
201 S University St.
West Lafayette, IN
Email: cottrellka@pudue.edu
Telephone: 765-494-6941

Jason D. Weber, Ph.D.
Department of Medicine
Division of Molecular Oncology
Washington University School of Medicine
660 South Euclid Avenue
Campus Box 8069
St. Louis, MO 63110 USA
Email: jweber@wustl.edu
Telephone: 314-747-3896
Fax: 314-362-0152

Abstract

Detection of viral double-stranded RNA (dsRNA) is an important component of innate immunity. However, many endogenous RNAs containing double-stranded regions can be misrecognized and activate innate immunity. The interferon inducible ADAR1-p150 suppresses dsRNA sensing, an essential function for ADAR1 in many cancers, including breast. Although ADAR1-p150 has been well established in this role, the functions of the constitutively expressed ADAR1-p110 isoform are less understood. We used proximity labeling to identify putative ADAR1-p110 interacting proteins in breast cancer cell lines. Of the proteins identified, the RNA helicase DHX9 was of particular interest. Knockdown of DHX9 in ADAR1-dependent cell lines caused cell death and activation of the dsRNA sensor PKR. In ADAR1-independent cell lines, combined knockdown of DHX9 and ADAR1, but neither alone, caused activation of multiple dsRNA sensing pathways leading to a viral mimicry phenotype. Together, these results reveal an important role for DHX9 in suppressing dsRNA sensing by multiple pathways.

Introduction

RNA editing enhances protein diversity and modulates multiple aspects of RNA metabolism[1–3]. A-to-I editing is carried out by adenosine deaminase acting on RNA 1 (ADAR1), an RNA editase that binds double-stranded RNA (dsRNA) and converts adenosines to inosines[4,5]. The main domains of ADAR1 include the Z-DNA binding domains (ZBD), the double-stranded RNA (dsRNA) binding domains (dsRBD), and the deaminase domain[6,7]. There are two isoforms, p110 and p150, produced by alternative transcriptional start sites[8]. They share the same deaminase domain, dsRBDs, and a ZBD, but exhibit a distinct subcellular localization[9,10]. ADAR1-p150 is predominantly cytoplasmic, whereas ADAR1-p110 is nuclear-localized[9,11].

An important role for ADAR1 is to suppress dsRNA sensing[12–15]. Many endogenously encoded RNAs can form large double-stranded regions, often through base-pairing between inverted Alu elements[16]. ADAR1 edits the majority of human genes, with most editing occurring within inverted Alu repeats[3,4]. By binding, editing, and thus altering the structure of dsRNA, ADAR1 suppresses the detection of dsRNA by various cytoplasmic sensors such as MDA5, RIG-I, and PKR[12,13,15,17]. These RNA sensors are part of innate immunity against viral infections[16,18–20]. Thus, ADAR1 prevents the activation of innate immunity pathways by endogenous immunogenic RNAs[16,19,21].

The cell-intrinsic antiviral response against foreign dsRNA - or misrecognized endogenous dsRNA - involves multiple pathways: (1) Recognition of dsRNA by MDA5 or RIG-I results in the activation of type I interferon (IFN-I) signaling[16,19,21]. (2) Activation of the dsRNA-binding kinase PKR triggers translational shutdown by phosphorylation of the translation initiation factor eIF2a[12]. (3) Detection of dsRNA by OAS proteins activates RNase L, which carries out non-specific cleavage of RNA and triggers cell death[22]. There is significant crosstalk between the three pathways, and the aforementioned dsRNA sensors are transcriptionally

controlled by IFN-I, known as interferon-stimulated genes (ISGs)[23,24]. The ADAR1-p150 isoform is itself an ISG and is the isoform responsible for suppressing the activation of dsRNA sensors[8,10,14,25]. ADAR1-p110, however, is constitutively expressed, though its functions are less established[26,27].

Because IFN-I signaling is often cytotoxic and antiproliferative, ADAR1's ability to suppress IFN-I signaling was shown to exert pro-tumor effects[21,28,29]. As such, ADAR1 has been proposed as a potential therapeutic target for various cancers, including breast cancer[28,30–32]. ADAR1 mRNA expression is elevated in breast cancer and is correlated with a poor prognosis[28,33]. Furthermore, ADAR1 is essential for a subset of breast cancer cells overrepresented by triple-negative breast cancer (TNBC)[33]. Known as 'ADAR1-dependency,' depletion of ADAR1-p150 leads to IFN-I signaling and global translational repression in cells that are sensitive to depletion of ADAR1[32,33]. What makes cancer cells sensitive or refractory to ADAR1 loss is not yet determined[33].

ADAR1 interacts with numerous RNA binding proteins including RNA helicases, transcription machinery, and DNA repair proteins [27,34–37]. The influence of ADAR1-interacting proteins on A-to-I editing has previously been reported[35,38–41]. In this study, we evaluated components of the ADAR1 interactome in breast cancer cells and identified the RNA helicase DHX9 as a redundant suppressor of immunogenic dsRNA in ADAR1-independent breast cancer cells. We demonstrate that co-depletion of ADAR1 and DHX9 is sufficient to trigger a viral mimicry phenotype in ADAR1-independent cells.

Results

Proximity Labeling by APEX2 Reveals ADAR1 Interacting Proteins

To better understand the role of ADAR1-p110 in breast cancer, we turned to a proximity labeling approach using APEX2 to identify putative ADAR1-p110-interacting proteins. Proximity labeling by APEX2 allows for the identification of proteins within 20 nm of an APEX2 fusion protein via biotin-mediated pulldown[42]. An APEX2-ADAR1-p110 fusion construct or APEX2 alone was expressed in MDA-MB-231, MCF-7, and SK-BR-3 (Fig. 1a). Following proximity labeling, biotinylated proteins were purified by streptavidin pulldown and subsequently identified by mass spectrometry (Fig 1b-c, Extended Data Fig. 1a, Supplementary Table 2). In total, we identified over one hundred enriched proteins across the three cell lines, with many identified in all three lines (Fig. 1d). Over-representation analysis of gene ontology (GO) terms revealed that many of the proteins identified by proximity labeling have roles in multiple aspects of RNA metabolism and localize to the nucleus and nucleolus (Fig. 1e, Supplementary Table 3). This finding was supported by a comparison to proteins previously observed to localize to the nucleus and nucleolus within MCF-7 in the SubCellBarcode dataset[43] (Fig.1f and 1g). These findings are largely consistent with the localization of ADAR1 within the cell lines studied. Immunofluorescence for ADAR1, which largely reflects the localization of ADAR1-p110 as the predominant isoform, showed that ADAR1 was localized in both the nucleus and nucleolus (Fig. 1h).

Validation of Protein Interactions Identified by Proximity Labeling

Although proximity labeling by APEX2 is a powerful technique for identifying putative protein-protein interactions, it does not distinguish between interactions and close associations[42]. To validate the proximity labeling findings and provide supporting evidence for direct protein-protein interactions, we performed co-immunoprecipitation followed by immunoblotting for five proteins identified by proximity labeling. ADAR1 could be immunoprecipitated by antibodies against the helicases DHX9, DDX17, and DDX54 (Fig. 2a-g). ADAR1 could also be immunoprecipitated with antibodies against XRN2 and PARP (Extended

Data Fig. 1b-c). To assess whether these potential interactions depended on RNA, we treated the lysates with RNase A to degrade RNA prior to immunoprecipitation (Extended Data Fig. 1d). Immunoprecipitation of ADAR1 by antibodies against DHX9, DDX17, and DDX54 was possible even in the presence of RNase A and improved in some cases (Fig. 2a-g). For DDX17 and DDX54, RNase A treatment did not change the co-immunoprecipitation results. However, DHX9 immunoprecipitated with both isoforms of ADAR1 in the absence of RNase A, but only with ADAR1-p110 when treated with RNase A. These findings suggest that DHX9, DDX17, and DDX54 directly interact with ADAR1-p110, and DHX9 interacts with ADAR1-p150 through an RNA bridge/scaffold. The co-immunoprecipitation findings are also consistent with the localization of the proteins studied. Much like ADAR1, the helicases DHX9, DDX17, and DDX54 localized to the nucleus or nucleolus (Fig. 2h-j). Together, these findings validate the results of the proximity labeling described in Fig. 1 and provide evidence for direct interactions between ADAR1 and multiple helicases.

DHX9 is overexpressed in breast cancer

Of the identified helicases, DHX9 was of particular interest for several reasons. First, DHX9 is the only helicase in humans that has a dsRBD. The dsRBD that is present in DHX9 is of the same class present in ADAR1 and PKR (Fig. 3a). Analysis of publicly available RNA-seq data for human cell lines and tumors revealed that DHX9 expression closely correlates with ADAR1 expression (Fig. 3b-d, Extended Data Fig. 2a-c). The correlation is stronger between DHX9 and the transcript encoding ADAR1-p110, than between DHX9 and ADAR1-p150 (Fig. 3c-d, Extended Data Fig. 2d-e). Furthermore, the expression of DHX9 and ADAR1 correlates better than any other helicase identified by proximity labeling (Fig. 3b, Extended Data Fig. 2b). Consistent with this correlated expression, and much like ADAR1, DHX9 is highly expressed in breast cancer and is correlated with a poor prognosis[33] (Fig. 3c, Extended Data Fig. 2f-h).

DHX9 is essential in TNBC cell lines and suppresses PKR activation

The similarities between ADAR1 and DHX9 led us to further study the role of DHX9 in breast cancer. Analysis of publicly available data from DepMap (https://depmap.org/portal/download/custom/) revealed that DHX9 is commonly essential in breast cancer cell lines (Fig. 3f). We validated this finding by knocking down DHX9 in four TNBC cell lines previously shown to be ADAR1-dependent[33]. In all four lines, knockdown of DHX9 caused cell death, likely through caspase-mediated apoptosis as indicated by cleaved PARP (Fig. 3g and h). Given the presence of the common dsRBD in DHX9 and PKR, and the role of DHX9 in regulating the abundance of dsRNA[44], we asked whether DHX9 could influence activation of PKR. To our surprise, we found that in three of the TNBC cell lines studied, knockdown of DHX9 caused activation of PKR (Fig. 3g and 3i). Together these findings show that DHX9 is essential in breast cancer cell lines and that in some ADAR1-dependent cell lines, DHX9 suppresses PKR activation.

DHX9 and ADAR1 redundantly suppress PKR activation

The experiments above were performed in ADAR1-dependent TNBC cell lines - cell lines that activate PKR following ADAR1 knockdown[33]. We were curious if DHX9 knockdown would also cause PKR activation in ADAR1-independent cell lines - cell lines that do not activate PKR following ADAR1 knockdown. Using shRNAs, we knocked down DHX9 in two ADAR1-independent breast cancer lines, MCF-7 and SK-BR-3 (Fig. 4a-b and 4f-g, Extended Data Fig. 4a-b and 4g-h). Unlike in ADAR1-dependent cell lines, knockdown of DHX9 did not cause activation of PKR in ADAR1-independent cell lines (Fig. 4a, 4d, 4f, 4i). Next, we asked whether combined knockdown of ADAR1 and DHX9 in these cell lines would lead to activation of PKR. As we had previously observed, knockdown of ADAR1 in SK-BR-3 and MCF-7 did not cause PKR activation[33]. However, combined knockdown of DHX9 and ADAR1 caused robust

activation of PKR in both cell lines (Fig. 4a, 4d, 4f, 4i). Consistent with PKR activation, we observed increased phosphorylation of the PKR substrate eIF2α following combined knockdown of ADAR1 and DHX9 (Fig. 4a and 4d, Extended Data Fig. 4c and 4i). Like in ADAR1-dependent TNBC cell lines, knockdown of DHX9 caused reduced proliferation of MCF-7 and SK-BR-3 (Fig. 4c, 4d, 4h, 4j), likely through caspase-dependent apoptosis, as indicated by elevated cleaved PARP (Fig. 4a, 4d, Extended Data Fig. 4e, 4k). Although PARP cleavage was increased upon combined knockdown of DHX9 and ADAR1, this did not statistically reduce the proliferation of the cells compared to single knockdown of ADAR1 and DHX9 as measured by foci formation. Together, these results reveal that ADAR1 and DHX9 redundantly suppress PKR activation in ADAR1-independent breast cancer cell lines.

DHX9 and ADAR1 redundantly suppress RNase L activation

Next, we wanted to evaluate the activation of other dsRNA sensing pathways in ADAR1-independent cell lines after the combined knockdown of ADAR1 and DHX9. To assess whether the IFN-I pathway, or other pathways, is activated after combined knockdown of ADAR1 and DHX9 we turned to analysis of differential gene expression by RNA-seq. In the process of preparing RNA for sequencing, we were surprised to find specific degradation of rRNA in MCF-7 cells following combined knockdown of ADAR1 and DHX9 (Fig. 4k). Single knockdown of either DHX9 or ADAR1 did not cause rRNA degradation. The observed rRNA degradation in the combined knockdown cells was reminiscent of the degradation products caused by RNase L[45]. Transfection with poly(I:C), which activates the IFN-I pathway and RNase L[46], created an identical band pattern to that of combined knockdown of DHX9 and ADAR1, indicating that the degradation of rRNA observed in these cells is likely caused by RNase L activity (Fig. 4k). We performed the same experiment with the ADAR1-dependent TNBC cell lines described above. In these cells, we did not see activation of RNase L after the knockdown of DHX9 alone (Extended Data 3h).

DHX9 and ADAR1 redundantly suppress multiple innate immunity pathways

RNA sequencing revealed that many more RNAs were differentially expressed after combined knockdown of DHX9 and ADAR1, compared to single knockdown of ADAR1 or DHX9 (Fig. 5a, Extended Data Fig. 5a-f). Analysis of differential gene expression by gene set enrichment after combined knockdown of ADAR1 and DHX9 in MCF-7 revealed activation of multiple pathways involved in the innate response to viral infection and repression of several pathways involved in translation (Fig. 5b and Supplemental Table 14). An enrichment map showed that the activated pathways associated with innate immunity formed one cluster and the depressed pathways formed a separate cluster (Extended Data Fig. 5g). Of the upregulated pathways, several were associated with activation of IFN signaling (Fig. 5b, and Supplementary Table 14). Analysis of core ISG expression revealed significant upregulation of ISGs in MCF-7 after combined knockdown of ADAR1 and DHX9 (Fig. 5c and Extended Data 5c). On the contrary, knockdown of DHX9 or ADAR1 alone did not increase ISG expression. Activation of RNase L described above also indicated that the type I IFN pathway was active in MCF-7 after double knockdown of DHX9 and ADAR1, because the activators of RNase L, the OAS proteins, are ISGs[22]. In fact, a GO term associated with OAS activity was upregulated in MCF-7 after combined knockdown of ADAR1 and DHX9 (Supplementary Table 14). Consistent with activation of PKR, we also observed increased expression of ATF4 targets (Fig. 5d) and NF-KB targets (Fig. 5e). Interestingly, we did not observe activation of any of these pathways or RNase L in SK-BR-3 following combined ADAR1 and DHX9 knockdown.

The finding that combined knockdown of ADAR1 and DHX9 did not induce ISG expression in SK-BR-3 is consistent with our findings in TNBC cell lines. While knockdown of DHX9 alone caused activation of PKR in several TNBC cell lines, we observed no activation of the type I IFN pathway, as indicated by no change in ISG15 expression (Extended Data Fig. 3f-g). ISG15 was found to be highly upregulated at the RNA and protein level in MCF-7 after

double knockdown of ADAR1 and DHX9 (Extended Data Fig. 4f, 4m, Supplementary Table 8). Like ISG expression overall, ISG15 expression in SK-BR-3 was not changed by knockdown of DHX9 and/or ADAR1 (Extended Data Fig. 4l, 4n).

Given the previously described role of DHX9 in the control of Alu containing RNAs, we next sought to assess if increased expression of transposable elements, especially Alus, could explain the activation of PKR or the IFN pathway upon combined knockdown of DHX9 and ADAR1. Analysis of our RNA-seq data revealed that transposable element expression was generally unchanged upon either single knockdown of ADAR1 or DHX9, or combined knockdown of both proteins (Extended Data Fig. 6a-f).

The dsRBDs of DHX9 are sufficient to suppress PKR activation in the absence of ADAR1

Having shown through knockdown studies that ADAR1 and DHX9 function redundantly to suppress dsRNA sensing, we next wanted to assess which functions of DHX9 and which isoforms of ADAR1 are important for this role. To determine which functions of DHX9 are sufficient to suppress PKR activation, we performed a rescue experiment with wild-type DHX9, a helicase deficient mutant DHX9, and a truncated DHX9 that possess the N-terminal dsRBDs fused to EGFP (Fig. 6a). Overexpression of wild-type DHX9 rescued the PKR activation phenotype caused by double knockdown of ADAR1 and DHX9, confirming that the observed phenotypes are not an off-target effect of the shRNAs used for knockdown (Fig. 6b and 6d). Interestingly, the DHX9^{K417R} mutant, which lacks helicase activity due to its inability to bind ATP[47], was also capable of suppressing PKR activation. The same was true for a construct which contained the dsRBDs of DHX9 fused to EGFP (dsRBD-EGFP). These findings indicate that the DHX9 dsRBDs are likely sufficient to suppress PKR activation in the absence of ADAR1 and DHX9. However, only wild-type DHX9 could rescue the reduced foci formation observed

after DHX9 knockdown (Fig. 6c and 6e). This finding indicates that the PKR activation phenotype and the reduced proliferation phenotype are uncoupled.

Consistent with the observation that the DHX9 dsRBDs are sufficient to suppress PKR activation, knockdown of DDX17, which lacks dsRBDs, did not cause substantial PKR activation in SK-BR-3 (Extended Data Fig. 9). Unlike DHX9, knockdown of DDX17 had no effect on cell proliferation as measured by the foci formation assay (Extended Data Fig. 9b and 9d). While combined knockdown of DHX9 and ADAR1 in SK-BR-3 caused a 5-10 fold increase in PKR phosphorylation, the combined knockdown of DDX17 and ADAR1 caused only a modest 1.5-fold increase in PKR phosphorylation (Extended Data Fig. 9a and 9c). This finding underscores the novel role of the DHX9 helicase and its dsRBD, a unique domain among this large family of RNA helicases.

The p110 and p150 isoforms of ADAR1 suppress PKR activation in the absence of DHX9

Next, we turned to ADAR1, and asked which isoform of ADAR1 is sufficient to suppress PKR activation in the absence of DHX9. We used the same approach as above, a rescue experiment with overexpression of ADAR1-p110 or ADAR1-p150. Interestingly, we found that both ADAR1 isoforms were sufficient to suppress PKR activation upon loss of DHX9 (Fig. 6f and 6h, Extended Data Fig. 8a-b). However, overexpression of neither ADAR1 isoform was able to rescue the foci formation phenotype, again indicating that the PKR activation and cell proliferation phenotypes are uncoupled (Fig. 6g and 6i).

Discussion

In recent years, ADAR1 has become an important therapeutic target for breast and other cancers. It is clear from the literature that depletion of ADAR1 in ADAR1-dependent cell lines leads to activation of dsRNA sensors and innate immunity programs that lead to cell death[21,32,33]. Yet unclear is what distinguishes ADAR1-dependent cell lines from ADAR1-

independent cell lines - those that are insensitive to ADAR1 depletion. Elevated ISG expression has been proposed as a potential prerequisite for ADAR1-dependency, but some ADAR1-independent cell lines exhibit elevated ISG expression[21,33]. As such, more information is needed to identify the factors that establish ADAR1-dependency or ADAR1-independency. To begin to fill in some of the knowledge gaps surrounding ADAR1, we utilized proximity labeling to identify putative ADAR1 interacting proteins, specifically focusing on the less studied ADAR1-p110 isoform.

Of the proteins identified by proximity labeling, the DEAH box helicase DHX9 was of particular interest. Like ADAR1 and PKR, DHX9 possesses dsRBDs, a singularly unique trait among the DEAD/DEAH box RNA helicase family. DHX9 expression is strongly correlated with ADAR1-p110 expression in breast cancer. Interestingly, both genes are located on the q-arm of chromosome 1, though they are separated by 28 mb and are thus unlikely to be physically co-regulated. Consistent with other reports in the literature, we show here that ADAR1 and DHX9 likely interact directly[38]. We observed that ADAR1-p110 and DHX9 interact in an RNA-independent manner, while the interaction between ADAR1-p150 and DHX9 was disrupted by RNase treatment. This result contradicts previous findings, in which ADAR1-p150 and DHX9 co-immunoprecipitated after RNase A treatment[44]. This discrepancy may be due to different cell lines used, HEK293T was used for the previous study, or different accessibility of DHX9 epitopes during immunoprecipitation. The importance of the ADAR1-DHX9 interaction is unclear from this work. Further studies are needed to structurally assess the interaction and directly perturb the interaction to understand what function it may have.

Here we report that in addition to being a commonly essential gene in breast cancer, DHX9 suppresses dsRNA sensing. In ADAR1-dependent cell lines, knockdown of DHX9 alone - much like knockdown of ADAR1 alone - caused activation of the dsRNA sensor PKR[33]. Like ADAR1 knockdown, DHX9 knockdown had no effect on PKR activation in ADAR1-independent cell lines. However, combined knockdown of DHX9 and ADAR1 caused robust activation of

PKR in these cells. This finding indicates that ADAR1 and DHX9 function redundantly to suppress PKR activation in ADAR1-independent cell lines and provides an explanation for why PKR is not activated in ADAR1-independent cells upon ADAR1 knockdown. Interestingly, like ADAR1, DHX9 has been shown to interact with PKR and is phosphorylated by PKR[48]. More research is needed to understand the importance of PKR phosphorylation of DHX9 and whether or not it may serve as a feedback mechanism.

Rescue experiments revealed that the helicase activity of DHX9 was dispensable for suppression of PKR activation. In fact, the N-terminal dsRBDs of DHX9 were sufficient to suppress PKR activation in the absence of ADAR1 in ADAR1-independent cell lines. This finding provides evidence for a model in which DHX9 competes with PKR for dsRNA binding through its dsRBDs (Fig. 7). This competition is likely to be indirect, as DHX9 is nuclear localized while PKR is generally localized in the cytosol[49–52]. As such, DHX9 may function to suppress PKR activation by sequestering dsRNAs in the nucleus.

Previously, the ADAR1 p150 isoform, and not the p110 isoform, was shown to be responsible for suppression of PKR activation. Through rescue experiments, we show here that both isoforms are sufficient to suppress PKR activation in the absence of DHX9 in ADAR1-independent cell lines. A preprint that was published during the preparation of this manuscript showed that the dsRBDs of ADAR1, ADAR2, and STAU1 were sufficient to suppress PKR activation[53]. Based on this finding and our rescue experiment with the DHX9 dsRBDs, it is likely that ADAR1-p150 and ADAR1-p110 suppress dsRNA sensing in the absence of DHX9 by competing with PKR for dsRNA binding. Although this may be direct competition in the case of ADAR1-p150 localized cytoplasmically, ADAR1-p110 may function like DHX9 to sequester dsRNAs in the nucleus.

In addition to suppression of PKR activation, we also observed that DHX9 and ADAR1 redundantly suppress activation of several other dsRNA sensing pathways in MCF-7. Knockdown of both proteins caused activation of IFN-I signaling, likely via MDA5 activation, as

322 previously shown for ADAR1[13,15]. We also observed activation of OAS-RNaseL and increased
323 expression of the ATF4 and NF-KB targets, likely downstream of PKR activation[54–56]. Taken
324 together, combined knockdown of DHX9 and ADAR1 in MCF-7 creates a viral mimicry
325 phenotype, where multiple innate immune pathways against RNA viruses have been activated
326 (Fig. 7). Interestingly, we only observed activation of PKR in other cell lines after either DHX9
327 knockdown alone or combined knockdown with ADAR1. Two possible explanations for this
328 discrepancy could be 1) Another factor may be present in some cells that suppresses dsRNA
329 sensing in the absence of DHX9 and/or ADAR1. 2) The expression of endogenous dsRNAs that
330 cause activation of sensors other than PKR may vary, leading to the differential effects of
331 ADAR1 and/or DHX9 knockdown. Further studies are needed to identify the immunogenic
332 RNAs that activate the various sensors.

333 Induction of viral mimicry has great potential as a therapeutic approach for multiple
334 cancers, including TNBC[57–60]. In addition to the cell intrinsic effects of activating innate immune
335 pathways within the tumor, the signaling that occurs after activation of those pathways can
336 promote anti-tumor immunity, especially when combined with checkpoint inhibitors[61–63].
337 Combined therapies targeting ADAR1 and DHX9 may serve as an effective means of treating
338 breast and other cancers by inducing viral mimicry.

339 **Materials and Methods**

340 **Cell culture**

341 Breast cancer cell lines (MCF-7 (RRID:CVCL_0031), SK-BR-3 (RRID:CVCL_0033), BT-
342 549 (RRID: CVCL_1092), MDA-MB-231 (RRID: CVCL_0062), HCC1806 (RRID: CVCL_1258),
343 MDA-MB-468 (RRID: CVCL_0063) and 293T (RRID: CVCL_0063) were obtained from
344 American Type Culture Collection. All cell lines were cultured in Dulbecco's modified Eagle's

medium (DMEM) (Hyclone) with 10% fetal bovine serum (Invitrogen), 2 mM glutamine (Hyclone), 0.1 mM nonessential amino acids (Hyclone), and 1 mM sodium pyruvate (Hyclone).

Viral Production and Transduction

Lentivirus was produced by Turbo DNAfection 3000 (Lamda Biotech) transfection of 293T cells with pCMV-VSV-G, pCMV-ΔR8.2, and the appropriate plasmid for expression of genes of interest or shRNAs. Virus was harvested 48 hours post-transfection. Cells were transduced with lentivirus for 16 hours in the presence of 10 µg/mL protamine sulfate (Sigma-Aldrich). The cells were selected with puromycin at 2 µg/mL (Sigma-Aldrich), 150 µg/mL hygromycin (Invitrogen) or 10 µg/mL Blasticidin (Invitrogen). The sequences for the shRNA-scramble (shSCR) and shRNA-ADAR1 (shADAR1) were described and validated previously[33]. The sequences for shRNAs against DHX9 and DDX17 are in Supplementary Table 1.

Plasmids

APEX2 was PCR amplified from pcDNA3-APEX2-NES, a kind gift from the laboratory of Kendall Blumer at Washington University in St. Louis. ADAR1-p110 was PCR amplified from pLVX-p110-ADAR1 described previously[33]. APEX2 and p110 were cloned into pLVX-IRES-puro (Takara, 632183) via a series of restriction enzyme digests and ligations. The final plasmids pLVX-3xFLAG-APEX2 and pLVX-3xFLAG-APEX2-linker-p110 were confirmed by digestion and sequencing. The linker consists of three repeats of Gly-Gly-Gly-Gly-Ser. Lentiviral shRNA constructs in the pLKO.1-puro vector were purchased as glycerol stocks from Millipore Sigma (Supplemental Table 1). For shADAR1, the shRNA was subcloned into pLKO.1-hygro (Addgene, #24150). Overexpression constructs for DHX9 and ADAR were generated by PCR amplification and ligation into pLV-EF1a-IRES-Blast vector (Addgene, #85133). For DHX9 overexpression, wobble mutants were made to reduce shRNA targeting. Mutagenesis primers for DHX9 K417R and shRNA-resistant codons (designed using the Synonymous Mutation

Generator[64]) are included in Supplemental Table 1. The DHX9-dsRBD-EGFP construct was generated by digestion of pLV-EF1-DHX9 with SpeI and EcoRI and ligation of EGFP in place of the 3' portion of DHX9. The resulting construct codes for the first 344 amino acids of DHX9 fused to EGFP.

Immunoblot

Cell pellets were lysed and sonicated in RIPA Buffer (50 mM Tris pH 7.4 (Ambion), 150 mM NaCl (Ambion), 1% Triton X-100 (Sigma-Aldrich), 0.1% sodium dodecyl sulfate (Sigma-Aldrich) and 0.5% sodium deoxycholate (Promega) with 1x HALT Protease Inhibitor (Pierce). Protein was quantified using the DC Assay kit (Bio-Rad) and diluted in SDS Sample Buffer (125 mM Tris pH 6.8, 30% glycerol, 10% sodium dodecyl sulfate, 0.012% bromophenol blue) prior to denaturation by heating to 95 °C for 7 minutes. Thirty micrograms of protein lysate were resolved on 4-12% TGX Acrylamide Stain-Free gels (Bio-Rad). Stain-Free gels were imaged prior to transfer to PVDF membrane (Millipore or Bio-Rad) by TransBlot Turbo (Bio-Rad). The blots were then probed with the appropriate primary antibodies: ADAR1 (Santa Cruz, sc-73408; Bethyl Laboratories, A303-883A), DDX17 (Thermo Scientific, PA5-84585), DHX9 (Bethyl, A300-855A), DDX54 (Novus Biologicals, NB100-60678), eIF2a (Abcam, ab5369), eIF2a-Ser-51-P (Abcam, ab32157), Fibrillarin (Santa Cruz, sc-25397), beta-tubulin (Abcam, ab6046), ISG15 (Santa Cruz, sc-166755), cleaved PARP (Cell Signaling, #9541), PKR (Cell Signaling, #3072), PKR Thr-446-P (Abcam, ab32036). Primary antibodies were detected with horseradish-peroxidase conjugated secondary antibodies (Jackson ImmunoResearch) and detection was carried out with Clarity Western ECL Substrate (Bio-Rad). Densitometry was performed using Image Lab (Bio-Rad). Band intensity was normalized to total protein measured by imaging of the Stain-Free gel.

Proximity Labeling by APEX2

SK-BR-3, MCF-7, or MDA-MB-231 cells expressing pLVX-puro-FLAG-APEX2 or pLVX-puro-FLAG-APEX2-ADAR1p110 were grown to ~80% confluency in a 15 cm dish. Quencher solution (10 mM sodium azide, 10 mM sodium ascorbate, and 5 mM Trolox (Sigma-Aldrich, 238813-1G) in 1X PBS) was prepared at 1X and 2X concentrations. Prior to labeling, cells were incubated in 10 mL of culture media containing 500 μM biotin phenol (Toronto Research Chemicals, B397770) for 30 min at 37 °C. Next, hydrogen peroxide was added to the cells at 1 mM and incubated at room temperature for 1 min. Immediately one volume of 2X quencher solution was added to the cells to stop labeling. The cells were washed twice with 1X quencher solution. Cells were harvested by scraping in 1X quencher solution and lysed in RIPA buffer containing 10 mM sodium azide, 10 mM sodium ascorbate, 5 mM Trolox and 1x HALT. Biotin labeling was verified by immunoblotting with HRP-streptavidin (Abcam, ab7403). Biotinylated proteins were purified using streptavidin magnetic beads (Thermo Fisher Scientific, 88816). Streptavidin magnetic beads were washed twice with RIPA containing HALT and quenching agents. The lysate from above was incubated with the beads for 1 hour at room temperature. The beads were washed in the following order: once with RIPA containing HALT and quenching agents, once with RIPA, once with 1 M KCl, once with 2 M urea pH 8.0, twice in RIPA and once with water. Elution was performed in 1X SDS-Sample buffer by heating at 95 °C for 10 minutes. The eluate was analyzed by LC-MS-MS, see below.

Mass Spectrometry

Liquid-chromatography and tandem mass spectrometry was performed by MSBioWorks (Ann Arbor, MI). The eluates from the streptavidin pulldown above were processed by SDS-PAGE using 10% Bis-Tris NuPage Mini-gel (Invitrogen) with the MES buffer system. The gel was run 2cm. The mobility region was excised and processed by in-gel digestion with trypsin using a robot (ProGest, DigiLab). For the trypsin digestion, the gel slices were washed with 25mM ammonium bicarbonate followed by acetonitrile. The samples were reduced with 10mM

dithiothreitol at 60°C followed by alkylation with 50mM iodoacetamide at room temperature. Subsequently proteins were digested with trypsin (Promega) at 37°C for 4 h. The trypsin digestion was quenched with formic acid and the supernatant was analyzed directly without further processing. The digested sample was analyzed by nano LC-MS/MS with a Waters M-Class HPLC system interfaced to a ThermoFisher Fusion Lumos mass spectrometer. Peptides were loaded on a trapping column and eluted over a 75 µm analytical column at 350 nL/min; both columns were packed with Luna C18 resin (Phenomenex). The mass spectrometer was operated in data-dependent mode, with the Orbitrap operating at 60,000 FWHM and 15,000 FWHM for MS and MS/MS respectively. APD was enabled and the instrument was run with a 3 s cycle for MS and MS/MS. Five hours of instrument time was used for the analysis of each sample.

Analysis of Mass Spectrometry Data

Data were searched using a local copy of Mascot (Matrix Science) with the following parameters: Enzyme - Trypsin/P; Database - SwissProt Human (concatenated forward and reverse plus common contaminants); Fixed modification – Carbamidomethyl; Variable modifications - Oxidation; Acetyl; Pyro-Glu; Deamidation; Mass values – Monoisotopic; Peptide Mass Tolerance - 10 ppm; Fragment Mass Tolerance - 0.02 Da; Max Missed Cleavages - 2. Mascot DAT files were parsed into Scaffold (Proteome Software) for validation, filtering and to create a non-redundant list per sample. Data were filtered using a 1% protein and peptide FDR and requiring at least two unique peptides per protein. Fold change of protein abundance was determined by DESeq2 using spectral counts (see Data Availability below for scripts). Overrepresentation analysis was performed using ‘enrichR’ in R[65]. The cutoff used for enrichment for the overrepresentation analysis was an FDR < 0.05 and a log2 fold change of > 0.5.

Immunoprecipitation

Cell lysates prepared in RIPA with 1X HALT. RNaseOUT (Thermo Fisher) RNase inhibitor was added to the lysis buffer at 0.5 U/µL when RNase A was not used. One milligram of protein lysate was mixed with 2-10 µg of IgG or specific antibody overnight at 4 °C with rotation. For samples treated with RNase A, 20 µg of RNase A (Invitrogen) was added to the lysate during overnight mixing with the antibody. Protein G Dynabeads (Thermo Fisher, 25 µL per sample) were prepared by washing twice in the lysis buffer. Prepared beads were mixed with lysates for 30 min at 4 °C with rotation. Supernatants were collected and beads were washed three times in the lysis buffer, and eluted by mixing the beads in SDS sample buffer and incubating at 95 °C for 7 min. Antibodies: Rabbit IgG (Jackson ImmunoResearch, 011-000-003), Mouse IgG (Jackson ImmunoResearch, 015-000-003), DHX9 (Bethyl, A300-855A), PARP (Cell Signaling, 9532S), XRN2 (Novus, NB100-57541), DDX54 (Novus, NB100-60678), DDX17 (Thermo Scientific, PA5-84585).

Immunofluorescence

Cells were plated on glass coverslips (Corning) two days prior to fixation for immunofluorescence. Cells were washed in PBS prior to fixation with 4% paraformaldehyde (Thermo Scientific) and permeabilization with 0.15% Triton-X100 in PBS. Following permeabilization the cells were washed three times with PBS then blocked with Protein Block (Aligent/Dako, X090930-2). Primary antibodies (ADAR1 (Santa Cruz, sc-73408), Fibrillarin (Santa Cruz, sc-25397), DDX54 (Novus Biologicals, NB100-60678) or DDX17 (Thermo Scientific, PA5-84585), DHX9 (Bethyl, A300-855A)) and secondary antibodies (Thermo Scientific, A21207, A21203, A21202, A21206) were diluted in Antibody Diluent (Agilent/Dako, S302283-2). Antibody binding was performed in a humidity chamber for 1.5 hours for primaries and 30 minutes for secondaries. Between primary and secondary antibodies, and after

secondary antibody binding the coverslips were washed in PBS. The coverslips were washed once in water before mounting on glass slides with Vectashield Antifade Mounting Media with DAPI (Vector Laboratories, H-1200-10). Fluorescence microscopy images were obtained with an Eclipse 90i microscope (Nikon) using a Plan Apochromatic 20x/NA 0.75 objective (Nikon) and a CoolSNAP ES2 monochrome digital camera cooled to 0°C (Photometrics). Fluorescence images were captured with MetaMorph version 7.8.0.0 software (Molecular Devices) and resized and formatted with Fiji.

Transfection of poly(I:C)

The cell line indicated was transfected with high-molecular weight poly(I:C) (Invivogen) with Lipofectamine LTX. Three microliters of Lipofectamine LTX was used per microgram of poly(I:C). Sixteen hours after transfection, cells were harvested in RIPA with 1X HALT or the RNA lysis buffer from the Nucleospin RNA kit (Macherey-Nagel).

RNA Purification and RNA sequencing

RNA-sequencing was performed for two replicates of ADAR1 and/or DHX9 knockdown in MCF-7 and SK-BR-3. RNA was purified using the Nucleospin RNA kit (Macherey-Nagel). Assessment of rRNA integrity and RNA-sequencing was performed by the Genome Technology Access Center at Washington University in St. Louis. Total RNA integrity was determined using Agilent TapeStation 4200. Library preparation was performed with 500 ng to 1 ug of total RNA. Ribosomal RNA was removed by an RNase-H method using RiboErase kit (Kapa Biosystems). After rRNA depletion, the remaining RNA was then fragmented in reverse transcriptase buffer (Life Technologies) by heating to 94 degrees for 8 minutes. The RNA was reverse transcribed to yield cDNA using SuperScript III RT and random hexamers (Life Technologies) per manufacturer's instructions. A second strand reaction was performed with DNA Polymerase I and RNase H (Qiagen) to yield ds-cDNA. The cDNA was then blunted with T4 DNA

Polymerase, Polynucleotide Kinase and Klenow DNA Polymerase (Qiagen). An A base was added to the 3' ends with Klenow (3'-4' exo-) (Qiagen). The processed ds-cDNA was then ligated to Illumina sequencing adapters with T4 DNA Ligase (Qiagen). Ligated fragments were then amplified for 12-15 cycles using primers incorporating unique dual index tags with VeraSeq polymerase (Qiagen). Fragments were sequenced on an Illumina NovaSeq-6000 using paired end reads extending 150 bases.

RNA Sequencing Analysis

The Illumina bcl2fastq software was used for base calling and demultiplexing, allowing for one mismatch in the indexing read. STAR version 2.7.9a1 was used for read alignment to RNA-seq to the Ensembl GRCh38.101 primary assembly. Gene counts were determined using Subread:featureCount version 2.0.32, only uniquely aligned unambiguous reads were counted. Differential gene expression was determined using DESeq2 (see Data Availability below for scripts)[66]. The experimental design for DESeq2 analysis included an interaction term between the shRNAs used for knockdown ('shrna1 + shrna2 + shrna1:shrna2'; where 'shrna1' was either shSCR or shADAR and 'shrna2' was either shSCR or shDHX9-3). Contrasts were used to assess differential expression after singular knockdown of either ADAR1 or DHX9. Fold changes were shrunken using the 'apeglm' approach from DESeq2[67]. Gene set enrichment analysis was performed using 'clusterProfiler'[68]. For analysis of transposable element expression, 'TEcount' from TEtranscripts[69] was used to determine family level counts for transposable elements using a GTF file containing transposable element information from RepeatMasker (http://www.repeatmasker.org). (see Data Availability section for more information about the GTF file).

Foci Formation Assay

Five thousand cells were plated for each condition in a 10 cm culture dish. After 10 (BT-549, MDA-MB-MB231, HCC1806, MDA-MB-468 and SK-BR-3) to 20 (MCF-7) days the cells were washed briefly with 1x PBS prior to fixation in 100% methanol for 5 min. After drying, the cells were stained with 0.005% Crystal Violet solution containing 25% methanol (Sigma-Aldrich) prior to washing excess stain away with deionized water. The plates were scanned using an ImageScanner III (General Electric). Foci area was calculated using ImageJ.

Analysis of CCLE and TCGA data

RNA-seq normalization and calculation of z-scores was performed as described previously[33]. Molecular subtypes of breast cancer cell lines and TCGA samples were defined previously[70]. Breast cancer survival analysis was performed using the R packages RTCGA and survminer[71,72]. The DHX9 expression level used for stratification in survival analysis was determine by the surv_cutpoint function of survminer.

Data and Code Availability

Scripts used for analysis of mass spectrometry, RNA-seq and generation of all plots are available at (https://github.com/cottrellka/Cottrell-Ryu-et-al-2023), raw sequencing data and count files were deposited at the Gene Expression Omnibus (GEO) under accession GSE224677. RNA-seq data for cancer cell lines (CCLE_expression_full.csv, CCLE_RNAseq_rsem_transcripts_tpm_20180929.txt) were obtained from the DepMap portal (https://depmap.org/portal/download/custom/)[73]. RNAi based dependency data for DHX9 (D2_combined_gene_dep_scores) was obtained from DepMap Portal (https://depmap.org/portal/download/custom/)[74]. RNA-seq data for TCGA BRCA samples (illuminahiseq_rnaseqv2-RSEM_genes, illuminahiseq_rnaseqv2-RSEM_isoforms_normalized) and clinical data (Merge_Clinical) were obtained from the Broad Institute FireBrowse and are available at http://firebrowse.org/. The GTF file used for TEcount

(GRCh38_Ensembl_rmsk_TE.gtf) is available at https://www.dropbox.com/sh/1ppg2e0fbc64bqw/AACUXf-TA1rnBIjvykMH2Lcia?dl=0.

Acknowledgements:

The authors would like to thank Leonard B. Maggi, Jr., Raleigh Kladney, Louis Kerestes, Che-Pei Kung, and Anbrielle Blake for technical assistance, Elliot Klotz and Toni Sinnwell (Genome Technology Access Center at Washington University) for RNA sequencing, Joshua B. Rubin, Jason C. Mills, Jieya Shao, and Alessandro Vindigni for discussion and suggestions. The data described here is in part based on data generated by the TCGA Research Network: https://www.cancer.gov/tcga. This work was supported by R01CA190986 (J.D.W.), K99MD016946 and R00MD016946 (K.A.C) from the National Institutes of Health, W81XWH-18-1-0025 (J.D.W.) and W81XWH-21-10466 (J.D.W.) from the Department of Defense, and a Centene Corporation Contract (P19-00559) for the Washington University–Centene ARCH Personalized Medicine Initiative (J.D.W.). L.S.T. supported by R25HG006687 and T32GM148405.

Author Contributions

K.A.C, S.R. and J.D.W. conceived the project. K.A.C., S.R., L.S.T., and A.M.S. performed the experiments. K.A.C., S.R., and L.S.T. performed the data analysis. K.A.C. and S.R. wrote the manuscript. All authors edited the manuscript.

Figure 1: Identification of putative ADAR1 interacting proteins by APEX2 proximity labeling

a Immunoblot showing expression of the constructs used for proximity labeling in MCF-7, MDA-MB-231 and SK-BR-3. **b** Representative fluorescently stained gel image showing proteins purified by streptavidin-biotin pulldown following proximity labeling in MCF-7. **c** Volcano plot summarizing the proteins identified by mass spectrometry following streptavidin pulldown subsequent to proximity labeling. Differential abundance of all proteins in each cell line can be found in Supplementary Table 2. **d** Venn diagram showing overlap between enriched proteins from all three cell lines. The cut-off for enriched proteins was an FDR adjusted p-value of less than 0.05 and a Log2 fold change of greater than 0.5. **e** GO terms found to be overrepresented in the list of the enriched proteins. Only the top ten GO terms, by FDR, are shown for each category. All other significant GO terms are available in the Supplementary Table 3-4. **f** and **g** Venn diagrams showing overlap between the enriched proteins identified and those proteins found previously to localize to the nucleus or nucleolus in MCF-7[43]. **h** Representative indirect immunofluorescence micrographs showing localization of ADAR1, fibrillarin (a nucleolar marker) and DAPI.

Figure 2: Validation of putative protein-protein interactions identified by proximity labeling

Immunoprecipitation of DHX9 **a**-**c**, DDX54 **d**-**e** or DDX17 **f**-**g** followed by immunoblot for ADAR in breast cancer cell lines**.** Immunoblot of immunoprecipitation eluates and inputs from SK-BR-3 **a**, **d** and **f**, MCF-7 **b**, **e** and **g**, and MDA-MB-231 **c**. Input represents 5% of the lysate used for immunoprecipitation. The IgG lanes represent immunoprecipitation eluates from pulldown with anti-rabbit IgG antibody. The lanes labeled DHX9, DDX54 and DDX17 indicate the eluates from immunoprecipitation with antibodies against those proteins respectively. The IgG^{HC} label indicates the band corresponding to the IgG heavy chain from the antibody used for immunoprecipitation. Uncropped immunoblots for panels **a**-**g** can be found in Source Data Figures. Immunofluorescence for ADAR1 and DHX9 **h**, DDX54 **i**, or DDX17 **j** in SKBR3 or MCF-7.

Figure 3: DHX9 is overexpressed in breast cancer and suppresses PKR activation

a Schematic showing the domain structure of PKR, ADAR1, DHX9 and other helicases identified by proximity labeling in Fig. 1, dsRBD refers to the dsRNA Binding Domain. **b** Pearson and Spearman correlation coefficients for the correlation between ADAR1 expression at the RNA level and the expression of each indicated helicase at the RNA level, data from breast tumors within TCGA. Scatterplots showing the correlation between ADAR1-p110 **c**, or ADAR1-p150 **d**, and DHX9 expression in normal breast or breast tumors. **e** Expression of DHX9 at the RNA level in normal breast, non-TNBC or TNBC tumors. **f** Waterfall plot showing DHX9 dependency of breast cancer cell lines using data from DepMap, ER = estrogen receptor positive cell lines, ERRB2 = HER2 positive cell lines. **g** Representative immunoblot following knockdown of DHX9 with two different shRNAs in four TNBC cell lines. Immunoblots for other replicates and uncropped blots can be found in Source Data Figures. **h** Foci formation assay for the same cells used in **g** for immunoblot. **i** Quantification of PKR phosphorylation as determined by the immunoblot in **g**. Quantification of protein expression for other proteins of interest can be found in Extended Data Fig. 3a-e. Bars represent the average of at least three replicates, error bars are +/- SD. * $p < 0.05$, ** $p < 0.01$, *** $p < 0.001$. P-values determined by Dunnett's test.

Figure 4: DHX9 and ADAR1 redundantly suppress dsRNA sensing in ADAR1-independent cell lines

Representative immunoblot showing the phenotype of ADAR1 and/or DHX9 knockdown in MCF-7 **a**, or SK-BR-3 **f**. Immunoblots for other replicates and uncropped blots can be found in Source Data Figures. Protein abundance from the immunoblot in **a** and **f** was normalized by total protein abundance by quantification of the Stain Free gel in **b** and **g** respectively. Fold change of PKR phosphorylation at Thr-446 in MCF-7 **d** or SK-BR-3 **i** as determined by the immunoblots in **a** or **f** respectively. Quantification of protein expression for other proteins of interest can be found in Extended Data Fig. 4a-l. Representative foci formation phenotype of ADAR1 and/or DHX9 knockdown in MCF-7 **c** or SK-BR-3 **h**, quantification of relative foci area is shown in **e** or **j** respectively. **k** Analysis of rRNA integrity upon knockdown of ADAR1 and/or DHX9 in MCF-7 or SK-BR-3. Additionally, panel **k** shows the effect of poly(I:C) (p(I:C)) transfection on rRNA integrity in MCF-7. Bars represent the average of at least three replicates, error bars are +/- SD. * $p < 0.05$, ** $p < 0.01$, *** $p < 0.001$. P-values determined by one-way ANOVA with post-hoc Tukey. Comparisons between the two different shRNAs targeting DHX9 (shDHX9-3 and shDHX9-5) were not included for clarity.

Figure 5: Induction of a viral mimicry phenotype upon knockdown of DHX9 and ADAR1 in MCF-7

A Volcano plot showing changes in RNA expression upon knockdown of DHX9 and ADAR1 in MCF-7, a volcano plot for SK-BR-3 is in Extended Data Fig. 5f. Fold-change of RNA expression shown in **a** was determined using an interaction term between ADAR1 and DHX9 knockdown, volcano plots for fold change of RNA expression for single knockdown of ADAR1 or DHX9 is in Extended Data Fig. 5a-b and 5d-e. **b** GO terms identified by gene set enrichment analysis of the RNA-seq data in **a**. **c**-**e** Heatmaps and summary box plots showing RNA expression changes in MCF-7 and SK-BR-3 upon knockdown of ADAR1 and/or DHX9. Panel **c** shows RNA expression for core ISGs[21,33], panel **d** shows ATF4 targets and panel **e** shows NF-KB targets with ISGs removed.

Figure 6: Rescue of PKR activation by ADAR1-p110, ADAR-p150, DHX9 and DHX9 mutants

a Schematic showing the domain structure of ADAR1 isoforms, DHX9 and mutants of DHX9, dsRBD refers to the dsRNA Binding Domain. Representative immunoblot showing the phenotype of ADAR1 and DHX9 knockdown with DHX9, DHX9^{K417R} or dsRBD-EGFP overexpression **b**, or ADAR1 isoform overexpression **f**. Immunoblots for other replicates and uncropped blots can be found in Source Data Figures. Fold change of PKR phosphorylation at Thr-446 upon ADAR1 and DHX9 knockdown with DHX9, DHX9^{K417R} or dsRBD-EGFP overexpression **d**, or ADAR1 isoform overexpression **h**, quantified from immunoblots in **b** and **f** respectively. Quantification of protein expression for other proteins of interest can be found in Extended Data Fig. 7b-f and 8a-f. Representative foci formation phenotype of ADAR1 and DHX9 knockdown with DHX9, DHX9^{K417R} or dsRBD-EGFP overexpression **c**, or ADAR1 isoform overexpression **g**. Quantification of relative foci area is shown in **e** or **i**, respectively. Bars represent the average of at least three replicates, error bars are +/- SD. * $p < 0.05$, ** $p < 0.01$, *** $p < 0.001$. P-values determined by Dunnett's test.

Figure 7: Model of ADAR1 and DHX9s roles in suppression of dsRNA sensing.

A hypothetical model based on published data and the findings presented here. Dashed lines indicate multiple steps. Lines marked with question marks are proposed and require further investigation. Created with BioRender.com

References

1. Paz-Yaacov, N. *et al.* Elevated RNA Editing Activity Is a Major Contributor to Transcriptomic Diversity in Tumors. *Cell Rep.* **13**, 267–276 (2015).
2. Walkley, C. R. & Li, J. B. Rewriting the transcriptome: adenosine-to-inosine RNA editing by ADARs. *Genome Biol.* **18**, 205 (2017).
3. Li, M. *et al.* Widespread RNA and DNA Sequence Differences in the Human Transcriptome. *Science* **333**, 53–58 (2011).
4. Bazak, L. *et al.* A-to-I RNA editing occurs at over a hundred million genomic sites, located in a majority of human genes. *Genome Res.* **24**, 365–376 (2014).
5. Wagner, R. W., Smith, J. E., Cooperman, B. S. & Nishikura, K. A double-stranded RNA unwinding activity introduces structural alterations by means of adenosine to inosine conversions in mammalian cells and Xenopus eggs. *Proc. Natl. Acad. Sci.* **86**, 2647–2651 (1989).
6. Kim, U., Wang, Y., Sanford, T., Zeng, Y. & Nishikura, K. Molecular cloning of cDNA for double-stranded RNA adenosine deaminase, a candidate enzyme for nuclear RNA editing. *Proc. Natl. Acad. Sci.* **91**, 11457–11461 (1994).
7. Herbert, A. *et al.* A Z-DNA binding domain present in the human editing enzyme, double-stranded RNA adenosine deaminase. *Proc. Natl. Acad. Sci.* **94**, 8421–8426 (1997).
8. George, C. X. & Samuel, C. E. Human RNA-specific adenosine deaminase ADAR1 transcripts possess alternative exon 1 structures that initiate from different promoters, one constitutively active and the other interferon inducible. *Proc. Natl. Acad. Sci.* **96**, 4621–4626 (1999).
9. Desterro, J. M. P. *et al.* Dynamic association of RNA-editing enzymes with the nucleolus. *J. Cell Sci.* **116**, 1805–1818 (2003).

10. Patterson, J. B. & Samuel, C. E. Expression and regulation by interferon of a double-stranded-RNA-specific adenosine deaminase from human cells: evidence for two forms of the deaminase. *Mol. Cell. Biol.* **15**, 5376–5388 (1995).
11. Eckmann, C. R., Neunteufl, A., Pfaffstetter, L. & Jantsch, M. F. The human but not the Xenopus RNA-editing enzyme ADAR1 has an atypical nuclear localization signal and displays the characteristics of a shuttling protein. *Mol. Biol. Cell* **12**, 1911–1924 (2001).
12. Chung, H. *et al.* Human ADAR1 Prevents Endogenous RNA from Triggering Translational Shutdown. *Cell* **172**, 811-824.e14 (2018).
13. Liddicoat, B. J. *et al.* RNA editing by ADAR1 prevents MDA5 sensing of endogenous dsRNA as nonself. *Science* **349**, 1115–1120 (2015).
14. Pestal, K. *et al.* Isoforms of the RNA editing enzyme ADAR1 independently control nucleic acid sensor MDA5-driven autoimmunity and multi-organ development. *Immunity* **43**, 933–944 (2015).
15. Mannion, N. M. *et al.* The RNA-Editing Enzyme ADAR1 Controls Innate Immune Responses to RNA. *Cell Rep.* **9**, 1482–1494 (2014).
16. Chen, Y. G. & Hur, S. Cellular origins of dsRNA, their recognition and consequences. *Nat. Rev. Mol. Cell Biol.* **23**, 286–301 (2022).
17. Yang, S. *et al.* ADAR1 Limits RIG-I RNA Detection and Suppresses IFN Production Responding to Viral and Endogenous RNAs. *J. Immunol. Baltim. Md 1950* **193**, 3436–3445 (2014).
18. Clerzius, G. *et al.* ADAR1 Interacts with PKR during Human Immunodeficiency Virus Infection of Lymphocytes and Contributes to Viral Replication. *J. Virol.* **83**, 10119–10128 (2009).
19. Quin, J. *et al.* ADAR RNA Modifications, the Epitranscriptome and Innate Immunity. *Trends Biochem. Sci.* **46**, 758–771 (2021).

20. Montavon, T. C. *et al.* Human DICER helicase domain recruits PKR and modulates its antiviral activity. *PLOS Pathog.* **17**, e1009549 (2021).
21. Liu, H. *et al.* Tumor-derived IFN triggers chronic pathway agonism and sensitivity to ADAR loss. *Nat. Med.* **25**, 95–102 (2019).
22. Li, Y. *et al.* Ribonuclease L mediates the cell-lethal phenotype of double-stranded RNA editing enzyme ADAR1 deficiency in a human cell line. *eLife* **6**, e25687 (2017).
23. Rath, S. *et al.* Concerted 2-5A-Mediated mRNA Decay and Transcription Reprogram Protein Synthesis in the dsRNA Response. *Mol. Cell* **75**, 1218-1228.e6 (2019).
24. Schoggins, J. W. & Rice, C. M. Interferon-stimulated genes and their antiviral effector functions. *Curr. Opin. Virol.* **1**, 519–525 (2011).
25. George, C. X., Das, S. & Samuel, C. E. Organization of the mouse RNA-specific adenosine deaminase Adar1 gene 5'-region and demonstration of STAT1-independent, STAT2-dependent transcriptional activation by interferon. *Virology* **380**, 338–343 (2008).
26. Sun, T. *et al.* Decoupling expression and editing preferences of ADAR1 p150 and p110 isoforms. *Proc. Natl. Acad. Sci.* **118**, e2021757118 (2021).
27. Shiromoto, Y., Sakurai, M., Minakuchi, M., Ariyoshi, K. & Nishikura, K. ADAR1 RNA editing enzyme regulates R-loop formation and genome stability at telomeres in cancer cells. *Nat. Commun.* **12**, 1654 (2021).
28. Fumagalli, D. *et al.* Principles Governing A-to-I RNA Editing in the Breast Cancer Transcriptome. *Cell Rep.* **13**, 277–289 (2015).
29. Kung, C.-P., Maggi, L. B. & Weber, J. D. The Role of RNA Editing in Cancer Development and Metabolic Disorders. *Front. Endocrinol.* **9**, (2018).
30. Paz, N. *et al.* Altered adenosine-to-inosine RNA editing in human cancer. *Genome Res.* **17**, 1586–1595 (2007).
31. Chan, T. H. M. *et al.* A disrupted RNA editing balance mediated by ADARs (Adenosine DeAminases that act on RNA) in human hepatocellular carcinoma. *Gut* **63**, 832–843 (2014).

32. Gannon, H. S. *et al.* Identification of ADAR1 adenosine deaminase dependency in a subset of cancer cells. *Nat. Commun.* **9**, 5450 (2018).
33. Kung, C.-P. *et al.* Evaluating the therapeutic potential of ADAR1 inhibition for triple-negative breast cancer. *Oncogene* **40**, 189–202 (2021).
34. Ota, H. *et al.* ADAR1 forms a complex with Dicer to promote microRNA processing and RNA-induced gene silencing. *Cell* **153**, 575–589 (2013).
35. Freund, E. C. *et al.* Unbiased Identification of trans Regulators of ADAR and A-to-I RNA Editing. *Cell Rep.* **31**, 107656 (2020).
36. Sakurai, M. *et al.* ADAR1 controls apoptosis of stressed cells by inhibiting Staufen1-mediated mRNA decay. *Nat. Struct. Mol. Biol.* **24**, 534–543 (2017).
37. Jimeno, S. *et al.* ADAR-mediated RNA editing of DNA:RNA hybrids is required for DNA double strand break repair. *Nat. Commun.* **12**, 5512 (2021).
38. Hong, H. *et al.* Bidirectional regulation of adenosine-to-inosine (A-to-I) RNA editing by DEAH box helicase 9 (DHX9) in cancer. *Nucleic Acids Res.* **46**, 7953–7969 (2018).
39. Rajendren, S. *et al.* A protein–protein interaction underlies the molecular basis for substrate recognition by an adenosine-to-inosine RNA-editing enzyme. *Nucleic Acids Res.* **46**, 9647–9659 (2018).
40. Sapiro, A. L. *et al.* Zinc Finger RNA-Binding Protein Zn72D Regulates ADAR-Mediated RNA Editing in Neurons. *Cell Rep.* **31**, 107654 (2020).
41. Shamay-Ramot, A. *et al.* Fmrp Interacts with Adar and Regulates RNA Editing, Synaptic Density and Locomotor Activity in Zebrafish. *PLOS Genet.* **11**, e1005702 (2015).
42. Lam, S. S. *et al.* Directed evolution of APEX2 for electron microscopy and proximity labeling. *Nat. Methods* **12**, 51–54 (2015).
43. Orre, L. M. *et al.* SubCellBarCode: Proteome-wide Mapping of Protein Localization and Relocalization. *Mol. Cell* **73**, 166-182.e7 (2019).

44. Aktaş, T. *et al.* DHX9 suppresses RNA processing defects originating from the Alu invasion of the human genome. *Nature* **544**, 115–119 (2017).
45. Iordanov, M. S. *et al.* Activation of p38 mitogen-activated protein kinase and c-Jun NH(2)-terminal kinase by double-stranded RNA and encephalomyocarditis virus: involvement of RNase L, protein kinase R, and alternative pathways. *Mol. Cell. Biol.* **20**, 617–627 (2000).
46. Burke, J. M., Gilchrist, A. R., Sawyer, S. L. & Parker, R. RNase L limits host and viral protein synthesis via inhibition of mRNA export. *Sci. Adv.* **7**, eabh2479 (2021).
47. Nakajima, T. *et al.* RNA helicase A mediates association of CBP with RNA polymerase II. *Cell* **90**, 1107–1112 (1997).
48. Sadler, A. J., Latchoumanin, O., Hawkes, D., Mak, J. & Williams, B. R. G. An Antiviral Response Directed by PKR Phosphorylation of the RNA Helicase A. *PLOS Pathog.* **5**, e1000311 (2009).
49. Fuchsová, B. & Hozák, P. The Localization of Nuclear DNA Helicase II in Different Nuclear Compartments Is Linked to Transcription. *Exp. Cell Res.* **279**, 260–270 (2002).
50. Jeffrey, I. W. *et al.* Nuclear localization of the interferon-inducible protein kinase PKR in human cells and transfected mouse cells. *Exp. Cell Res.* **218**, 17–27 (1995).
51. García, M. A. *et al.* Impact of protein kinase PKR in cell biology: from antiviral to antiproliferative action. *Microbiol. Mol. Biol. Rev. MMBR* **70**, 1032–1060 (2006).
52. Lee, T. & Pelletier, J. The biology of DHX9 and its potential as a therapeutic target. *Oncotarget* **7**, 42716–42739 (2016).
53. ADAR1p150 Prevents MDA5 and PKR Activation via Distinct Mechanisms to Avert Fatal Autoinflammation | bioRxiv. https://www.biorxiv.org/content/10.1101/2023.01.25.525475v1.
54. Harding, H. P. *et al.* Regulated Translation Initiation Controls Stress-Induced Gene Expression in Mammalian Cells. *Mol. Cell* **6**, 1099–1108 (2000).
55. Pakos-Zebrucka, K. *et al.* The integrated stress response. *EMBO Rep.* **17**, 1374–1395 (2016).

56. Zamanian-Daryoush, M., Mogensen, T. H., DiDonato, J. A. & Williams, B. R. G. NF-κB Activation by Double-Stranded-RNA-Activated Protein Kinase (PKR) Is Mediated through NF-κB-Inducing Kinase and IκB Kinase. *Mol. Cell. Biol.* **20**, 1278–1290 (2000).
57. Roulois, D. *et al.* DNA-Demethylating Agents Target Colorectal Cancer Cells by Inducing Viral Mimicry by Endogenous Transcripts. *Cell* **162**, 961–973 (2015).
58. Chen, R., Ishak, C. A. & De Carvalho, D. D. Endogenous Retroelements and the Viral Mimicry Response in Cancer Therapy and Cellular Homeostasis. *Cancer Discov.* **11**, 2707–2725 (2021).
59. Jansz, N. & Faulkner, G. J. Endogenous retroviruses in the origins and treatment of cancer. *Genome Biol.* **22**, 147 (2021).
60. Wu, Q. *et al.* PRMT inhibition induces a viral mimicry response in triple-negative breast cancer. *Nat. Chem. Biol.* **18**, 821–830 (2022).
61. Zhou, X. *et al.* Pharmacologic Activation of p53 Triggers Viral Mimicry Response Thereby Abolishing Tumor Immune Evasion and Promoting Antitumor Immunity. *Cancer Discov.* **11**, 3090–3105 (2021).
62. Sheng, W. *et al.* LSD1 Ablation Stimulates Anti-tumor Immunity and Enables Checkpoint Blockade. *Cell* **174**, 549-563.e19 (2018).
63. Goel, S. *et al.* CDK4/6 inhibition triggers anti-tumour immunity. *Nature* **548**, 471–475 (2017).
64. Ong, J. Y. Synonymous Mutation Generator: a web tool for designing RNAi-resistant sequences. 2021.01.02.425100 Preprint at https://doi.org/10.1101/2021.01.02.425100 (2021).
65. Kuleshov, M. V. *et al.* Enrichr: a comprehensive gene set enrichment analysis web server 2016 update. *Nucleic Acids Res.* **44**, W90–W97 (2016).
66. Love, M. I., Huber, W. & Anders, S. Moderated estimation of fold change and dispersion for RNA-seq data with DESeq2. *Genome Biol.* **15**, 550 (2014).

67. Zhu, A., Ibrahim, J. G. & Love, M. I. Heavy-tailed prior distributions for sequence count data: removing the noise and preserving large differences. *Bioinforma. Oxf. Engl.* **35**, 2084–2092 (2019).

68. Wu, T. *et al.* clusterProfiler 4.0: A universal enrichment tool for interpreting omics data. *Innov. Camb. Mass* **2**, 100141 (2021).

69. Jin, Y., Tam, O. H., Paniagua, E. & Hammell, M. TEtranscripts: a package for including transposable elements in differential expression analysis of RNA-seq datasets. *Bioinforma. Oxf. Engl.* **31**, 3593–3599 (2015).

70. Marcotte, R. *et al.* Functional Genomic Landscape of Human Breast Cancer Drivers, Vulnerabilities, and Resistance. *Cell* **164**, 293–309 (2016).

71. Kosinski, M., Biecek, P. & Chodor, W. RTCGA: The Cancer Genome Atlas Data Integration. (2022) doi:10.18129/B9.bioc.RTCGA.

72. Kassambara, A., Kosinski, M., Biecek, P. & Fabian, S. survminer: Drawing Survival Curves using ‘ggplot2’. (2020).

73. Ghandi, M. *et al.* Next-generation characterization of the Cancer Cell Line Encyclopedia. *Nature* **569**, 503–508 (2019).

74. DepMap 22Q4 Public. (2022) doi:10.6084/m9.figshare.21637199.v2.

Figure 1

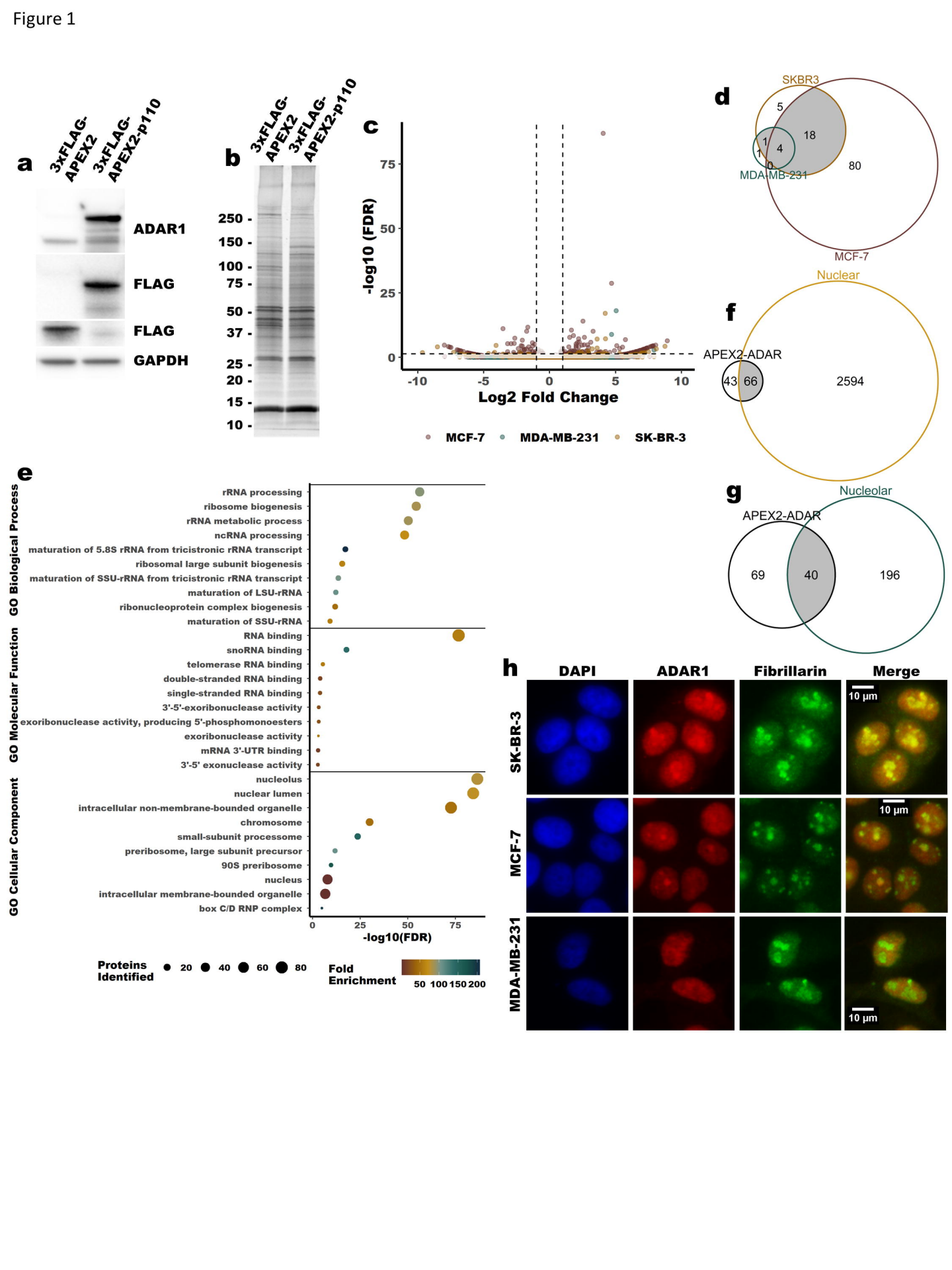
a
3xFLAG-APEX2
3xFLAG-APEX2-p110
ADAR1
FLAG
FLAG
GAPDH
b
3xFLAG-APEX2
3xFLAG-APEX2-p110
250
150
100
75
50
37
25
20
15
10
c
-log10 (FDR)
Log2 Fold Change
MCF-7
MDA-MB-231
SK-BR-3
d
SKBR3
MDA-MB-231
MCF-7
5
18
1
1
4
0
80
f
Nuclear
APEX2-ADAR
43
66
2594
g
Nucleolar
APEX2-ADAR
69
40
196
e
GO Biological Process
rRNA processing
ribosome biogenesis
rRNA metabolic process
ncRNA processing
maturation of 5.8S rRNA from tricistronic rRNA transcript
ribosomal large subunit biogenesis
maturation of SSU-rRNA from tricistronic rRNA transcript
maturation of LSU-rRNA
ribonucleoprotein complex biogenesis
maturation of SSU-rRNA
GO Molecular Function
RNA binding
snoRNA binding
telomerase RNA binding
double-stranded RNA binding
single-stranded RNA binding
3'-5'-exoribonuclease activity
exoribonuclease activity, producing 5'-phosphomonoesters
exoribonuclease activity
mRNA 3'-UTR binding
3'-5' exonuclease activity
GO Cellular Component
nucleolus
nuclear lumen
intracellular non-membrane-bounded organelle
chromosome
small-subunit processome
preribosome, large subunit precursor
90S preribosome
nucleus
intracellular membrane-bounded organelle
box C/D RNP complex
-log10(FDR)
Proteins Identified
20
40
60
80
Fold Enrichment
50
100
150
200
h
DAPI
ADAR1
Fibrillarin
Merge
SK-BR-3
MCF-7
MDA-MB-231
10 µm

Figure 2

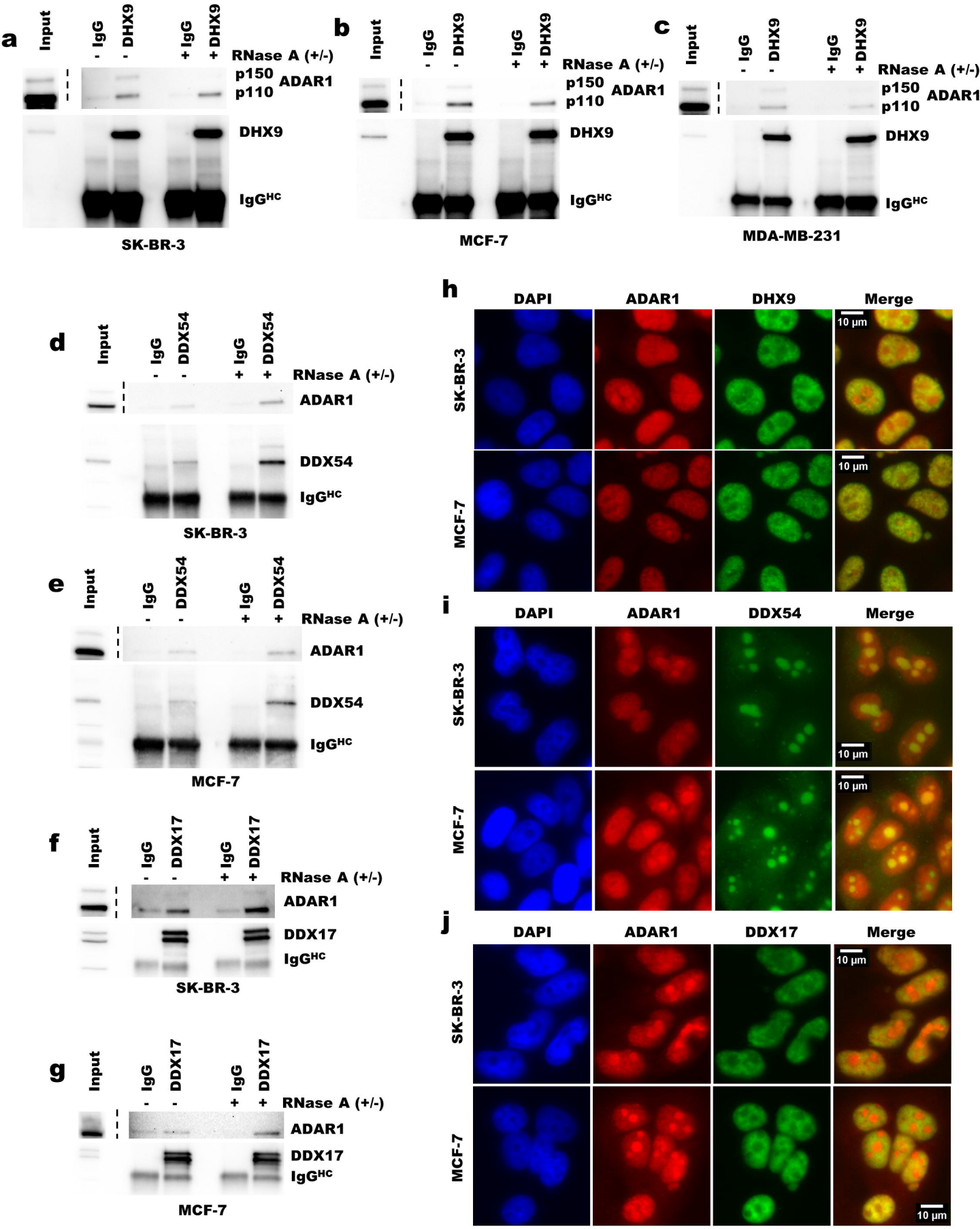
a
Input
- IgG
- DHX9
+ IgG
+ DHX9
RNase A (+/-)
p150
p110
ADAR1
DHX9
IgG^HC
SK-BR-3
b
Input
- IgG
- DHX9
+ IgG
+ DHX9
RNase A (+/-)
p150
p110
ADAR1
DHX9
IgG^HC
MCF-7
c
Input
- IgG
- DHX9
+ IgG
+ DHX9
RNase A (+/-)
p150
p110
ADAR1
DHX9
IgG^HC
MDA-MB-231
d
Input
- IgG
- DDX54
+ IgG
+ DDX54
RNase A (+/-)
ADAR1
DDX54
IgG^HC
SK-BR-3
e
Input
- IgG
- DDX54
+ IgG
+ DDX54
RNase A (+/-)
ADAR1
DDX54
IgG^HC
MCF-7
f
Input
- IgG
- DDX17
+ IgG
+ DDX17
RNase A (+/-)
ADAR1
DDX17
IgG^HC
SK-BR-3
g
Input
- IgG
- DDX17
+ IgG
+ DDX17
RNase A (+/-)
ADAR1
DDX17
IgG^HC
MCF-7
h
DAPI
ADAR1
DHX9
Merge
SK-BR-3
MCF-7
10 µm
i
DAPI
ADAR1
DDX54
Merge
SK-BR-3
MCF-7
10 µm
j
DAPI
ADAR1
DDX17
Merge
SK-BR-3
MCF-7
10 µm

Figure 3

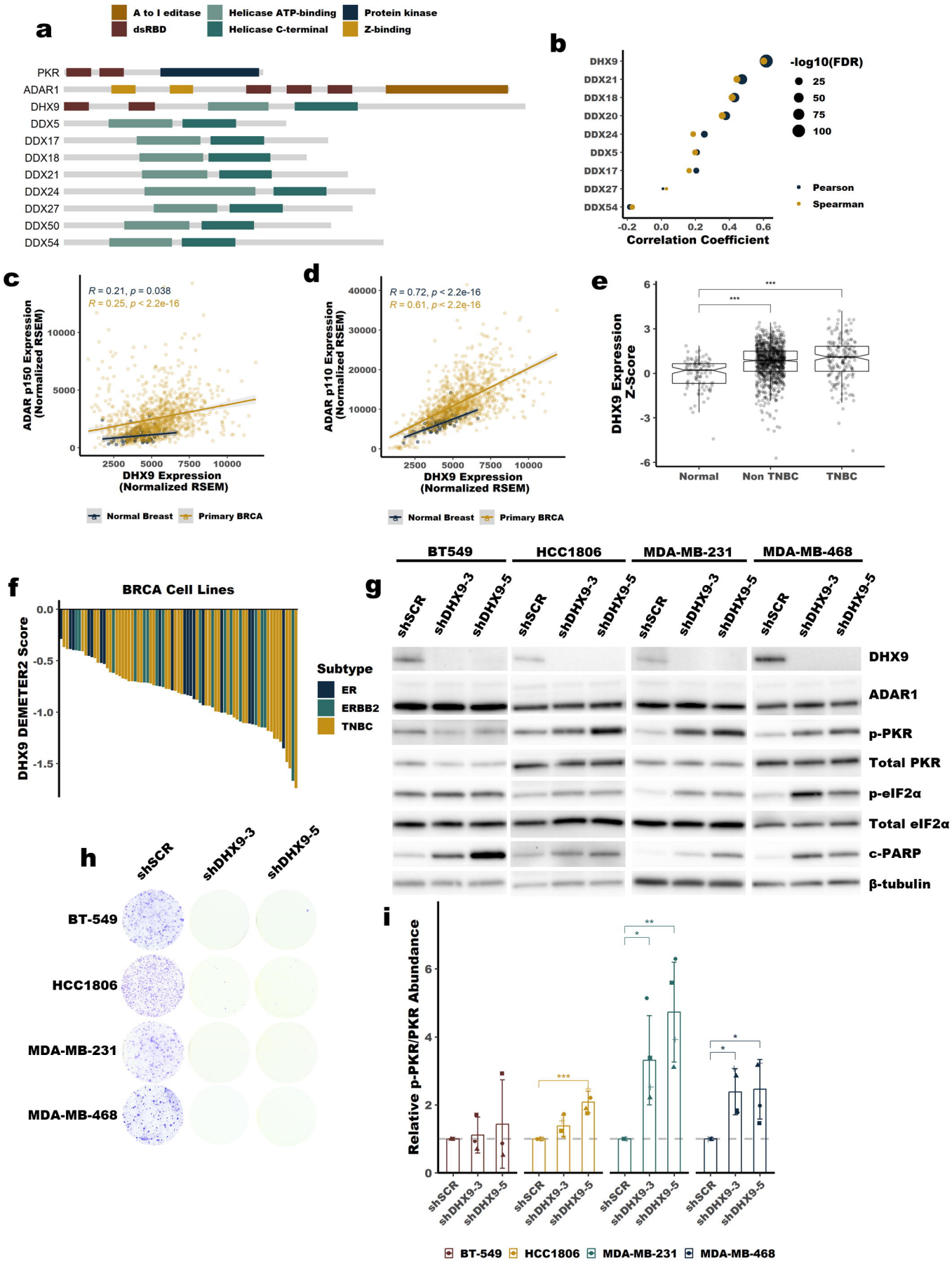
a
A to I editase
dsRBD
Helicase ATP-binding
Helicase C-terminal
Protein kinase
Z-binding
PKR
ADAR1
DHX9
DDX5
DDX17
DDX18
DDX21
DDX24
DDX27
DDX50
DDX54
b
-log10(FDR)
25
50
75
100
Pearson
Spearman
Correlation Coefficient
c
R = 0.21, p = 0.038
R = 0.25, p < 2.2e-16
ADAR p150 Expression (Normalized RSEM)
DHX9 Expression (Normalized RSEM)
Normal Breast
Primary BRCA
d
R = 0.72, p < 2.2e-16
R = 0.61, p < 2.2e-16
ADAR p110 Expression (Normalized RSEM)
DHX9 Expression (Normalized RSEM)
Normal Breast
Primary BRCA
e
DHX9 Expression Z-Score
Normal
Non TNBC
TNBC
f
BRCA Cell Lines
DHX9 DEMETER2 Score
Subtype
ER
ERBB2
TNBC
g
BT549
HCC1806
MDA-MB-231
MDA-MB-468
shSCR
shDHX9-3
shDHX9-5
DHX9
ADAR1
p-PKR
Total PKR
p-eIF2α
Total eIF2α
c-PARP
β-tubulin
h
shSCR
shDHX9-3
shDHX9-5
BT-549
HCC1806
MDA-MB-231
MDA-MB-468
i
Relative p-PKR/PKR Abundance
BT-549
HCC1806
MDA-MB-231
MDA-MB-468

Figure 4

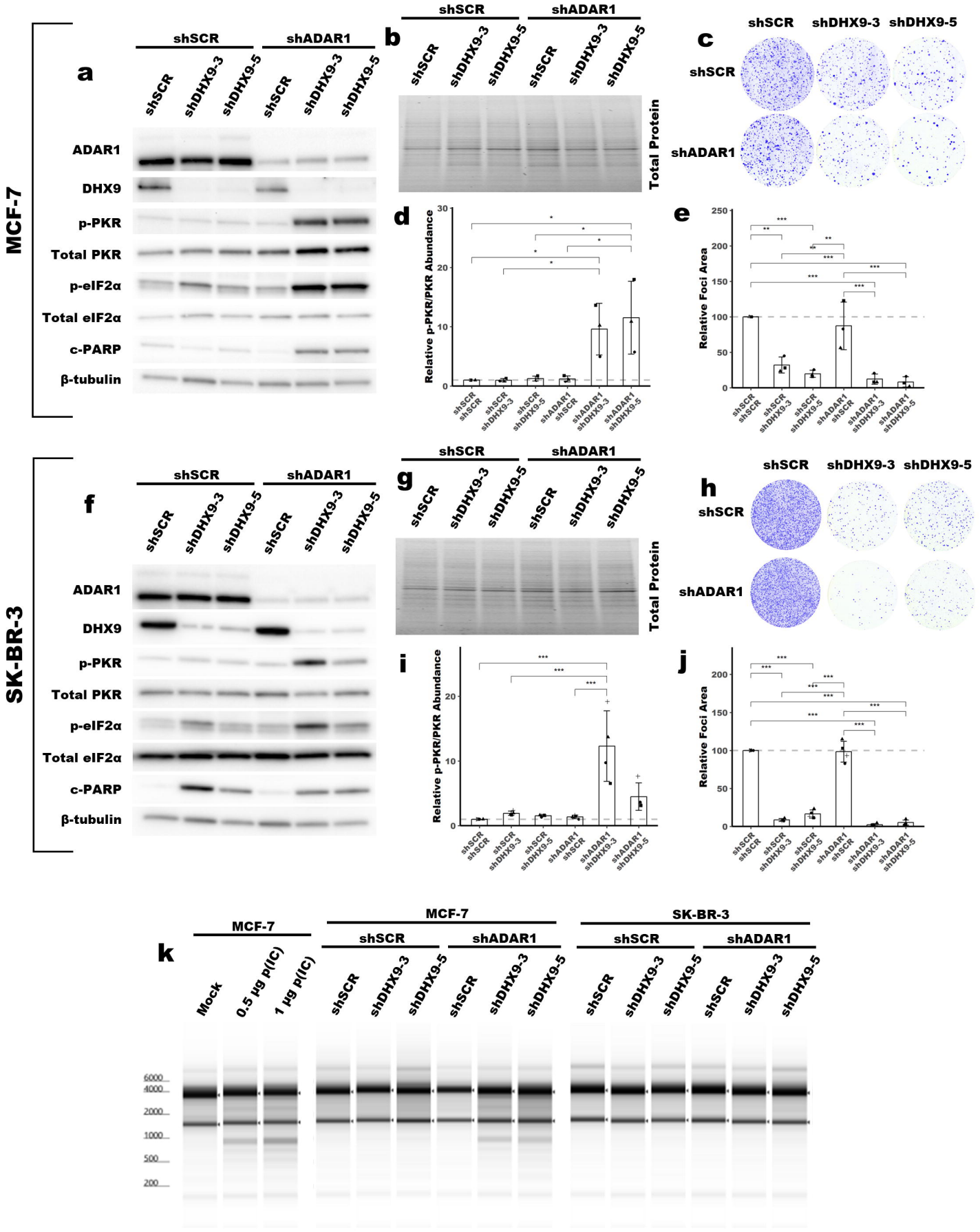
MCF-7
SK-BR-3
a
b
c
d
e
f
g
h
i
j
k
shSCR
shADAR1
shDHX9-3
shDHX9-5
ADAR1
DHX9
p-PKR
Total PKR
p-eIF2α
Total eIF2α
c-PARP
β-tubulin
Total Protein
Relative p-PKR/PKR Abundance
Relative Foci Area
Mock
0.5 µg p(IC)
1 µg p(IC)
6000
4000
2000
1000
500
200

Figure 5

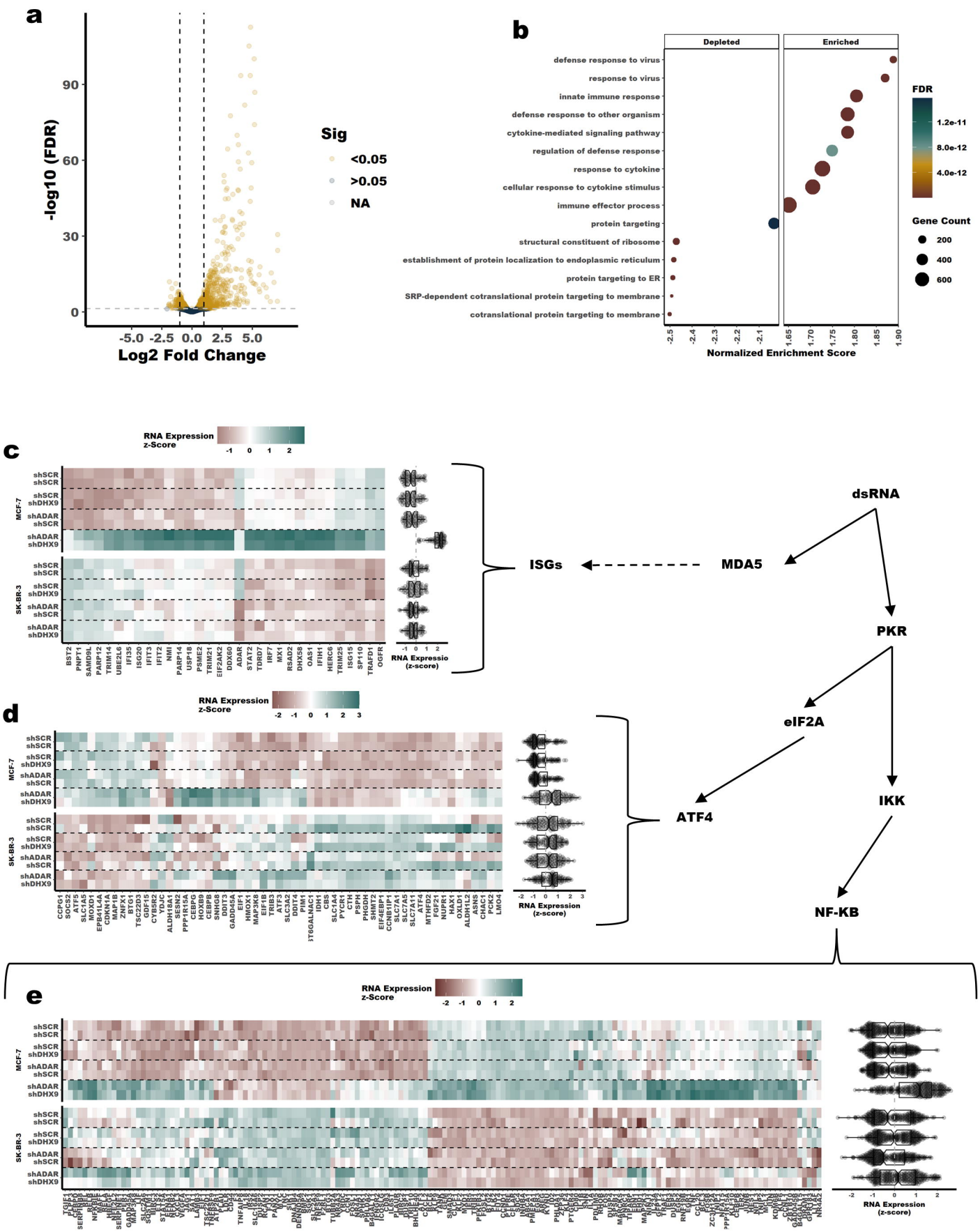
a
-log10 (FDR)
Log2 Fold Change
Sig
<0.05
>0.05
NA
b
Depleted
Enriched
defense response to virus
response to virus
innate immune response
defense response to other organism
cytokine-mediated signaling pathway
regulation of defense response
response to cytokine
cellular response to cytokine stimulus
immune effector process
protein targeting
structural constituent of ribosome
establishment of protein localization to endoplasmic reticulum
protein targeting to ER
SRP-dependent cotranslational protein targeting to membrane
cotranslational protein targeting to membrane
Normalized Enrichment Score
FDR
Gene Count
c
RNA Expression z-Score
MCF-7
SK-BR-3
shSCR
shADAR
shDHX9
RNA Expressio (z-score)
d
RNA Expression z-Score
RNA Expression (z-score)
e
RNA Expression z-Score
RNA Expression (z-score)
dsRNA
MDA5
ISGs
PKR
eIF2A
IKK
ATF4
NF-KB

Figure 6

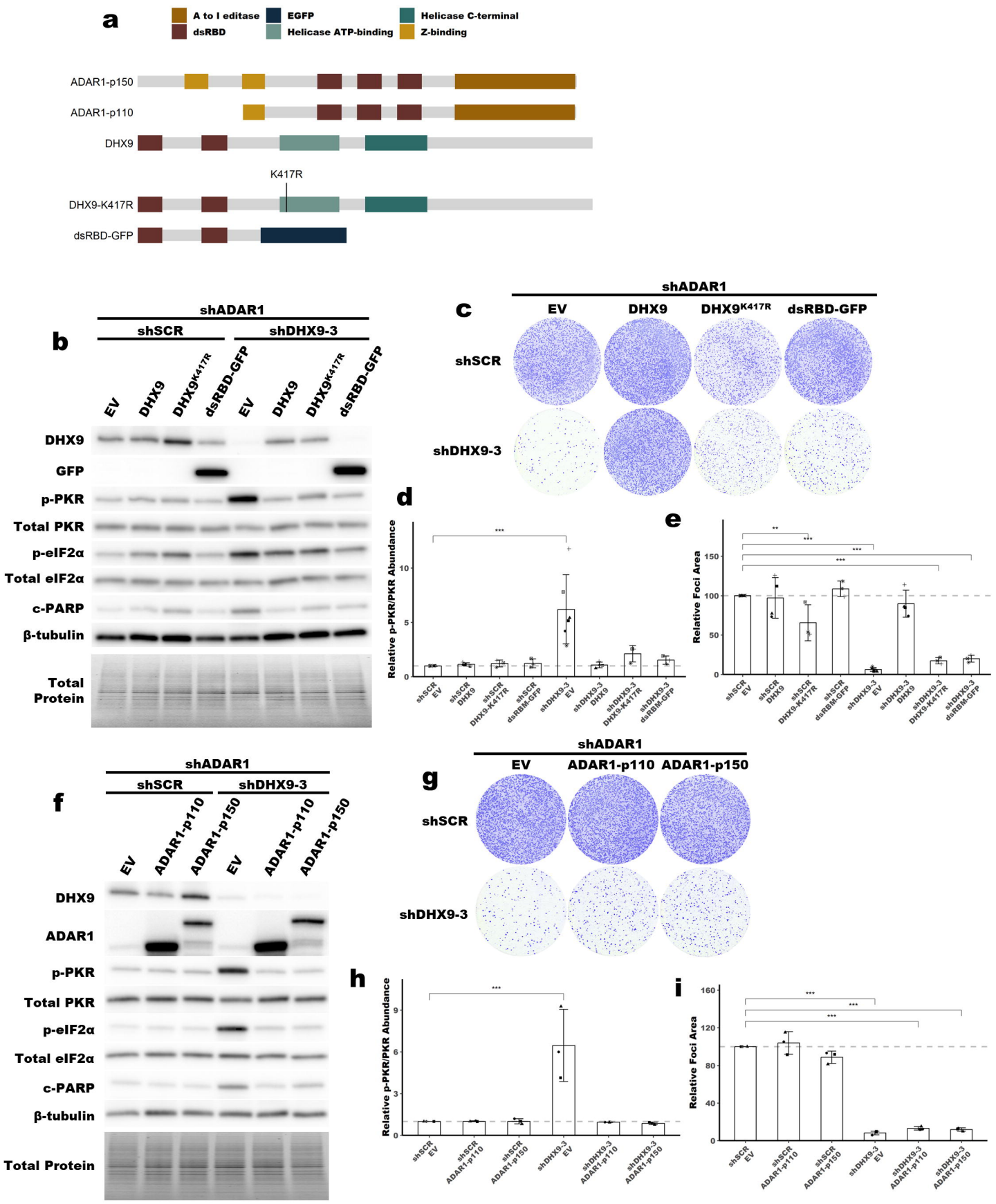
a
A to I editase
dsRBD
EGFP
Helicase ATP-binding
Helicase C-terminal
Z-binding
ADAR1-p150
ADAR1-p110
DHX9
K417R
DHX9-K417R
dsRBD-GFP
b
shADAR1
shSCR
shDHX9-3
EV
DHX9
DHX9K417R
dsRBD-GFP
DHX9
GFP
p-PKR
Total PKR
p-eIF2α
Total eIF2α
c-PARP
β-tubulin
Total Protein
c
shADAR1
EV
DHX9
DHX9K417R
dsRBD-GFP
shSCR
shDHX9-3
d
Relative p-PKR/PKR Abundance
e
Relative Foci Area
f
shADAR1
shSCR
shDHX9-3
EV
ADAR1-p110
ADAR1-p150
DHX9
ADAR1
p-PKR
Total PKR
p-eIF2α
Total eIF2α
c-PARP
β-tubulin
Total Protein
g
shADAR1
EV
ADAR1-p110
ADAR1-p150
shSCR
shDHX9-3
h
Relative p-PKR/PKR Abundance
i
Relative Foci Area

Figure 7

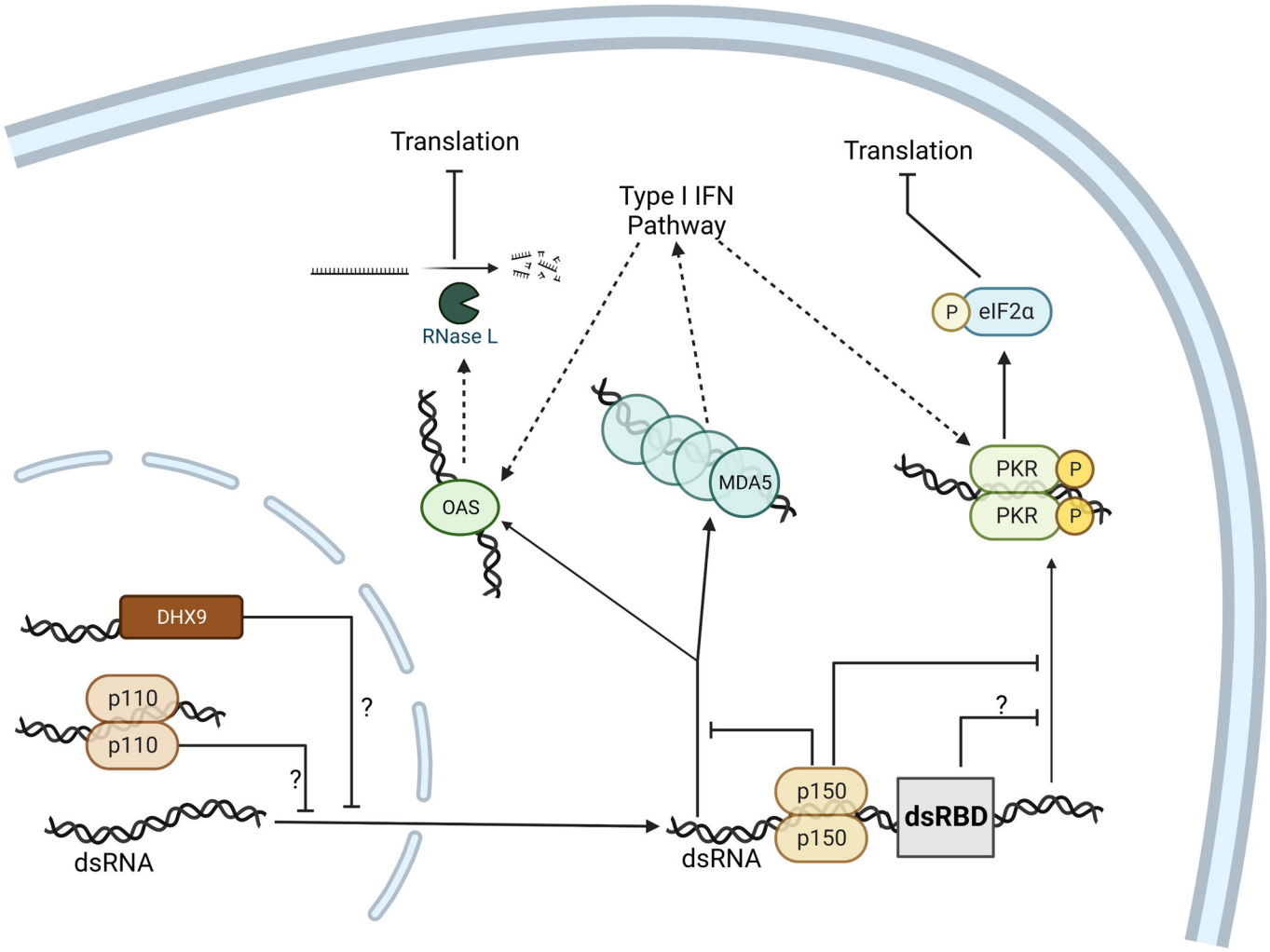
Translation
Translation
Type I IFN
Pathway
RNase L
P
eIF2α
OAS
MDA5
PKR
P
PKR
P
DHX9
p110
p110
?
?
?
dsRNA
p150
p150
dsRBD
dsRNA